MDPI

*Article*

# Experimental Study on the Effect of Steel Reinforcement Ration on the Cracking Behaviour of FRP-Strengthened RC Elements

Andrea Armonico [1], Laurent Michel [1], Mohamed Saidi [2] and Emmanuel Ferrier [1,*]

[1] Laboratory of Composite Materials for Construction (LMC2), University Claude Lyon 1, 82 bd Niels Bohr, 69622 Villeurbanne, France; andrea.armonico@univ-lyon1.fr (A.A.); laurent.michel@univ-lyon1.fr (L.M.)
[2] LOCIE, Université Savoie Mont-Blanc, Boulevard du Lac, 73370 Le Bourget-du-Lac, France; mohamed.saidi@univ-smb.fr
[*] Correspondence: emmanuel.ferrier@univ-lyon1.fr

**Abstract:** This paper examines the cracking behaviour of reinforced concrete beams strengthened by externally bonded fiber-reinforced polymer. The crack opening of RC structures is a key parameter for the durability of concrete structures. It is of vital importance for designers to be able to make correct estimations of the crack opening values of strengthened structures. FRP strengthening affects the cracking behaviour of RC beams with different steel percentages. Beams have been tested under four-point bending mechanical tests until failure with three steel ratios and two layers of externally bonded wet carbon fibers (CFRP). In order to measure the crack opening during loading, Digital Image Correlation is used to obtain the crack opening along the beam during load functioning. The results allow for a comparison of the RC beams with and without FRP and enhance the effect of FRP on crack opening. The crack width was compared with the theoretical values obtained based on the relation proposed by Eurocode 2 (EC2). The comparison enhanced the need to propose a modified relation. Subsequently, an empirical model was established as a modification of EC2, considering the presence of a CFRP system. The corresponding results were compared and discussed to validate the model. For the same level of loads, the crack opening can be reduced by 20 to 50% depending on the level of steel ratio.

**Keywords:** CFRP; digital image correlation; cracking; RC beams; strengthening

## 1. Introduction

In the past century, concrete structures have been used worldwide. The aging process of concrete and the upgrade of loading conditions have enhanced the need to strengthen these structures [1–6]. Since the 1990s, many structures have been strengthened to face these problems using externally bonded material, such as steel cladding and fiber-reinforced polymer. In the past 20 years, there has been an important research development in fiber-reinforced polymer (FRP) systems that are bonded in different forms (i.e., rebars, plates, fabrics, and grids) and with different fibers (i.e., carbon, glass, and aramid). These materials have several advantages including high strength, low weight, and excellent resistance to external agents [7]. Carbon fibers are preferred because of their properties and advantages compared with other synthetic fiber composites, such as higher mechanical properties, more excellent fatigue resistance, corrosion resistance, and creep resistance [8]. The main advantage is that to increase the tension capacity of a beam, the FRP material acts like an additional tension reinforcement; this allows for a slight improvement in the bending stiffness and the ultimate load [9–13]. These systems improve the capacity of RC elements with an increase in ductility and a limit in crack openings. Based on 30 years of research, several design codes and testing procedures have been developed [14–17]. This research has shown that failures in strengthened RC beams are obtained after large deflections and steel rebars yielding with FRP debonding. This debond can occur in the concrete part of the beam through intermediate debonding or through peeling-off at the end of the plate [18].

In a beam strengthened by FRP, researchers have enhanced that crack behavior is modified, crack spacing is modified with more small cracks in between the large cracks, and crack opening is also modified. Based on this development, an improvement of the strengthening technic has been performed with prestress FRP [11]. In this purpose anchorage system, a prestress process has been developed with excellent results [11]. However, this technique is not commonly used in the field because the process is not easy to implement in reality.

For durability purposes, the crack opening reduction is important to quantify. These effects have not been studied deeply in the literature; thus, it is necessary to conduct intense research to provide data that propose a design model suitable for RC strengthened by FRP.

At the same time, Digital Image Correlation has been developed in the construction industry, in order to measure displacements or deflections, or to localize the presence of cracks in reinforced concrete.

The feasibility of using an optical full-field Digital Image Correlation (DIC) technique for the measurement of strain fields on FRP materials used in the civil engineering industry has been investigated and the level of error in the DIC method when using more traditional methods was determined by Del Rey Castillo et al. [19]. The main advantage of using DIC over more traditional methods is the capacity to measure full field strains instead of strains at local points, which has been enhanced by providing the measurements of various specimens of FRP materials [20]. The reported strain fields are examples of what were obtained during an experimental campaign to understand the behavior of strengthened beams using externally bonded CFRP [21–23].

The present research program enhances changes in the mechanical behaviour of RC beams strengthened by externally bonded FRP systems and focuses on crack opening using DIC methods. The FRP considered in this study is a wet lay-up applied carbon sheet of 200 g/m$^2$. Three sets of beams were prepared with steel ratios of 0.4%, 0.6%, and 0.8%. These three levels of steel ratio correspond to structures with very low, low, and normal steel ratio reinforcement in building structures. The CFRP is applied by the wait lay-up method. The cross-section of the CFRP is fixed to 16.9 mm$^2$, based on the Young modulus of Carbon fibers (245 GPa) and the literature review. The FRP strengthening ratio is high enough to obtain a real strengthening effect on RC beams whatever the level of the steel ratio. The effects of applying two layers of CFRP were evaluated and discussed in detail regarding the influence of the steel ratio using beams tested for four-point bending.

Herein, the first section discusses the experimental program with material characterization and specimen setup. Next, the results are reviewed and deep analysis is performed on the changes in cracking behaviour, strength improvement, and midspan deflection.

The last section proposes the model based on the Eurocode 2 [24] formula, which is appropriately fitted for unstrengthened RC elements. In addition, the experimental and calculated results are compared and discussed, and some perspectives are provided.

## 2. Experimental Program

Ten RC beams with rectangular cross-sections of 150 by 250 mm are strengthened using two layers of CFRP sheets. Two layers have been retained in this study since, normally, 1 to 6 layers of CFRP can be added to RC structures, based on previous researchers' experience. Two layers of CFRP corresponds to a normal strengthening ratio.

### 2.1. Materials

The concrete used in this study has a characteristic concrete strength of C30/37, based on European standard [24].

### 2.1.1. Reinforced Concrete

The beams were cast using concrete with a characteristic compressive strength ($f_{ck}$) of 35 MPa as measured during the compression tests. The concrete mixtures used for the beam casting are listed in Table 1.

**Table 1.** Concrete composition.

| Component | Cement CEM I 52.5 R | Sand | Gravel | Water |
|:---:|:---:|:---:|:---:|:---:|
| [kg/m$^3$] | 420 | 890 | 890 | 200 |

The compression tests on the concrete were performed according to the NF EN 12390-1 standard [25]. The standard specifies the size of the specimens, limiting conditions, test velocity, and test procedure. The results are shown in Table 2 below.

**Table 2.** Concrete strength.

| Specimen | 1 | 2 | 3 | 4 | 5 | 6 | Average | Standard Deviation |
|:---:|:---:|:---:|:---:|:---:|:---:|:---:|:---:|:---:|
| σ [MPa] at 28 days | 37.4 | 38.2 | 42.2 | 38.65 | 38.85 | 44.1 | 39.9→35 | 2.41 |

The steel reinforcement consists of high limiting S500B rebar, having a characteristic yield strength ($f_{yk}$) of 500 MPa.

2.1.2. CFRP Reinforcement Material

The elastic modulus ($E_f$) of carbon sheet was 245 GPa, whereas the composite single-layer thickness was 0.169 mm, as reported in the technical datasheets provided by the manufacturer (Fibre NET, Pavia di Udine (UD), Italy). The FRP was applied by wet lay-up method of CFRP fabrics bonded using a bicomponent epoxy resin. The beams were retrofitted using a carbon-fiber-reinforced polymer consisting of unidirectional carbon fabric Betontex FB-GV330U-HT produced by Fiber Net s.p.a. The layers had a nominal thickness of 0.169 mm and Young's modulus ($E_f$) of 245 GPa, as reported in the technical datasheets provided by the manufacturer. The fibers were glued using a bicomponent epoxy resin Betontex FB-RC02 with a declared Young's modulus ($E_m$) of 3000 MPa and an ultimate strain equal to 2.9%. To verify the material properties, tests were performed, and results are given in Table 3. The elastic modulus was evaluated following the NF EN ISO 527-5 standard [26]; test coupons were prepared with 2-layer of CFRP fabrics. Uniaxial traction tests were performed using a universal testing machine (UTM). The tensile strength and Young modulus are reported in Figure 1 and Table 3, respectively, based on a calculation with an equivalent cross-section of the carbon fiber (thickness equal to 0.338 mm).
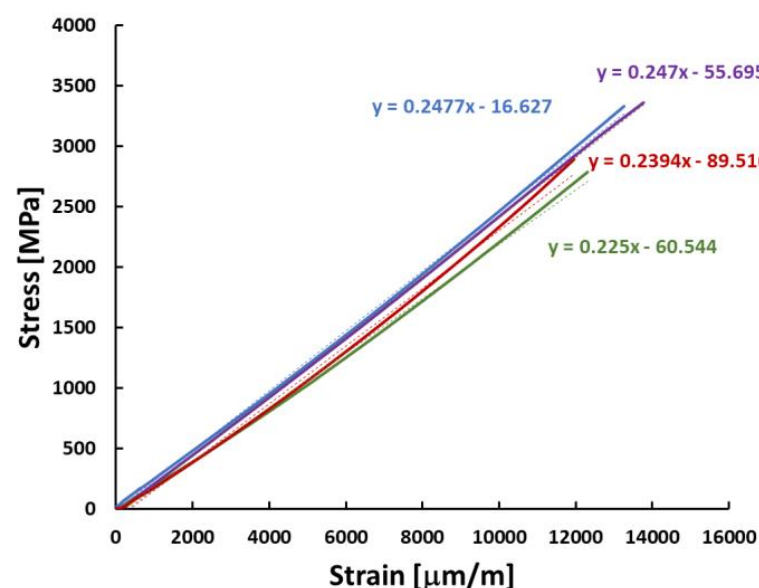


**Figure 1.** Uniaxial stress/strain behaviour of 2-layer CFRP sheets.

**Table 3.** Mechanical properties of 2-layer CFRP sheet.

| Specimen | Young's Modulus—$E_f$ [MPa] | Maximal Strain—$\varepsilon_u$ [%] | Ultimate Stress—$f_{tk}$ [MPa] |
|---|---|---|---|
| 1 | 225,000 | 1.23% | 2786.4 |
| 2 | 247,000 | 1.38% | 3363.4 |
| 3 | 242,200 | 0.88% | 2141.2 |
| 4 | 247,700 | 1.28% | 3329.5 |
| 5 | 239,400 | 1.20% | 2891.3 |
| **Average** | 240,260 | 1.19% | 2902.4 |
| **Standard deviation** | 9194.45 | 0.0018 | 496.99 |
| **Coeff. of variation** | 4% | 16% | 17% |

### 2.2. Specimen Preparation

The concrete mix was used to prepare ten RC beams with a rectangular cross-section of 150 mm × 250 mm, a 2.00-m span, and two reinforcing steel bars. The beams were prepared with different steel percentages: (i) 10 mm-diameter bars; (ii) 12 mm-diameter bars; and (iii) 14 mm-diameter bars, and hence steel ratios of 0.41%, 0.60%, and 0.82%. Details of the specimens are provided in Table 4.

**Table 4.** Specimen naming.

| Specimen Name | R10-NR * | R12-NR | R14-NR | R10-RB ** | R12-RB0 | R12-RB1 | R12-RB2 | R12-RB3 | R12-RB4 | R14-RB |
|---|---|---|---|---|---|---|---|---|---|---|
| Diameter of reinforcing bars | 10 | 12 | 14 | 10 | 12 | 12 | 12 | 12 | 12 | 14 |
| Presence of CFRP | No | No | No | Yes | Yes | Yes | Yes | Yes | Yes | Yes |

* RXNR: Rebars × mm Non-Reinforced. ** RXRBY Rebars × mm Reinforced before loading number Y.

Before bonding the composite layers, the beam's bottom surface was mechanically grouted and then a first layer of polymer was applied to improve CFRP adhesive performance onto the concrete. (Figure 2) The CFRP had a total final length equal to 1.9 m to avoid having CFRP on the bearing support during the test.



(**a**)                    (**b**)
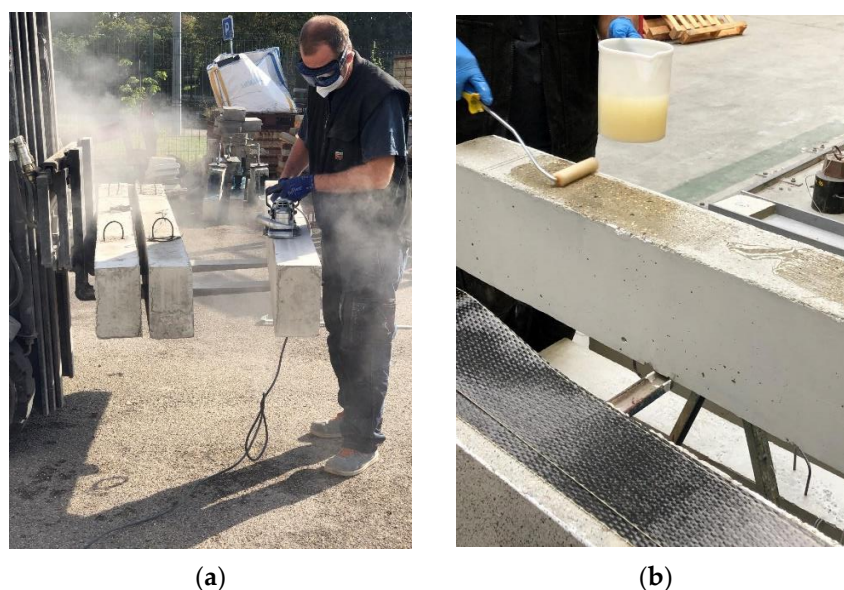
**Figure 2.** *Cont.*

(**c**)

**Figure 2.** Strengthening procedure. (**a**) Surface preparation. (**b**) First layer of polymer application. (**c**) CFRP sheet applied on support with a last layer of epoxy.

For each configuration, a beam was non-reinforced to be used as a reference. The test set up is reported in Figure 3.
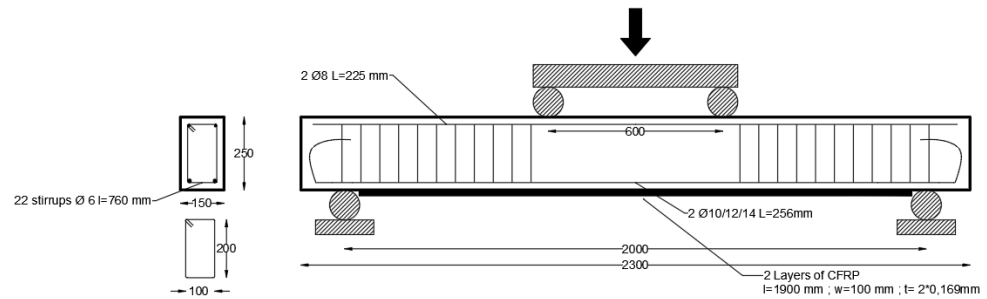


**Figure 3.** Beam setup.

Strain sensors were placed in the central area on longitudinal steel rebar and on the CFRP after the full polymerization of the CFRP.

The vertical displacement was monitored by two linear variable displacement transducers (LVDTs) placed in the mid part of the beam (Figure 4).
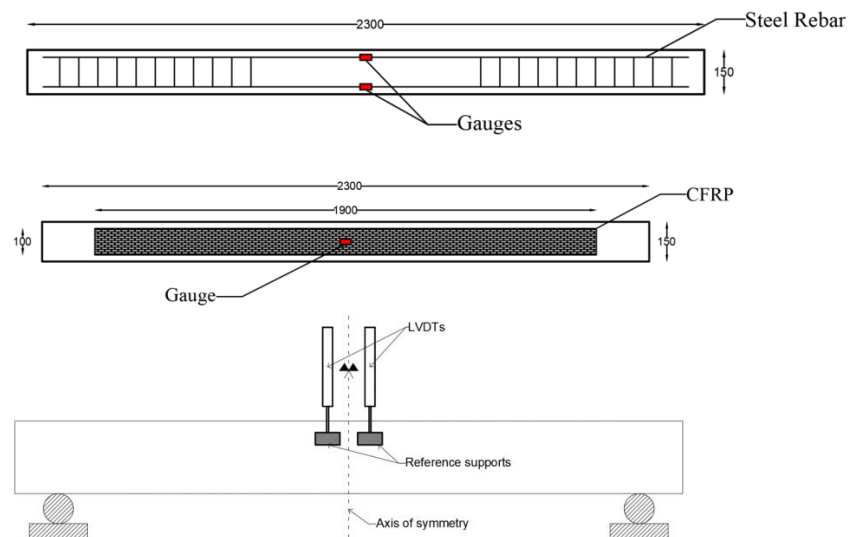


**Figure 4.** Strain gauge and LVDT location.

2.2.1. Two-Dimensional Digital Image Correlation (DIC 2D)

The crack was measured on the lateral surface of the beam in the middle where there is only normal stress without shear. The measurement techniques were based on the comparison of two images at two different levels of load. This noncontact optical technique was based on the theory of field displacement correlation to detect changes in pixel positions in a comparison of two stages (i.e., displacements or deformations) through consecutive image comparison. The surfaces of the specimens must be prepared with a white background and black speckles [27,28]. The image acquisition procedure was performed according to good practice for the DIC [29]. During the loading of beams, a set of data was obtained with several grayscale photos captured using a standard high resolution camera and a commercial correlation tools named GOM Correlate software 2015 was employed for post-processing [30]. The software algorithm requires the definition of a region of interest (ROI). There are several small facets called areas of interest (AOI) with well-defined pixel sizes [31]. The camera used was a Kramer electronics VP 211K with a resolution of $2560 \times 2048$ pixels$^2$ and a lens KOWA LM25HC:f = 25 mm; F 1.8–16. The focal was between f/6 and f/9. The size of measurement (ROI) was 600 mm $\times$ 250 mm. The density of the speckles was a fundamental factor in the accuracy of the results, which was related to the camera's proximity and resolution. Generally, as a guideline, A. D. Terani [29] suggests using 5-pixel size speckles covering 50% of the investigated surface. The tested specimens were inspected using the commercial software GOM Correlate®, which can process a set of 2D images by defining a scale factor, an ROI, and several AOIs. The size in pixels of the area of interest was equal to 30 px, with the distance of 20 px between their middles. The size of the AOI was directly proportional to the speckle dimension (large speckles correspond to large AOIs). Each AOI had a centre with a spatial location, which was used as a reference for the following steps. The axial strain ($\varepsilon_x$) or longitudinal displacement field map was obtained by comparing two images (see Figure 5). In Figure 5b, red values correspond to 2 mm and blue values to less than 0.02 mm.
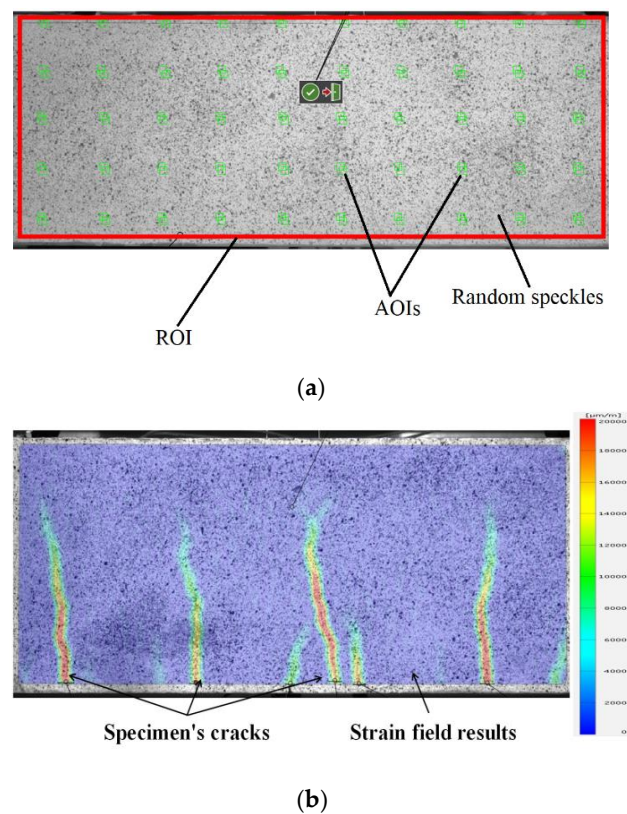


(**a**)



(**b**)

**Figure 5.** DIC procedure: (**a**) definition of ROI and AOIs; (**b**) strain map with crack locations.

### 2.2.2. Loading Device

The test set-up is based on a high stiffness steel frame equipped with a hydraulic jack which has a load capacity of 200 kN. The beams were simply supported, and their spans were 2 m. A four-point load was applied in the middle with a force distance of 600 mm [32–35]. Tests were performed using a displacement control system at a rate of 1 mm/min in isostatic conditions. The complete setup is illustrated in Figure 6.
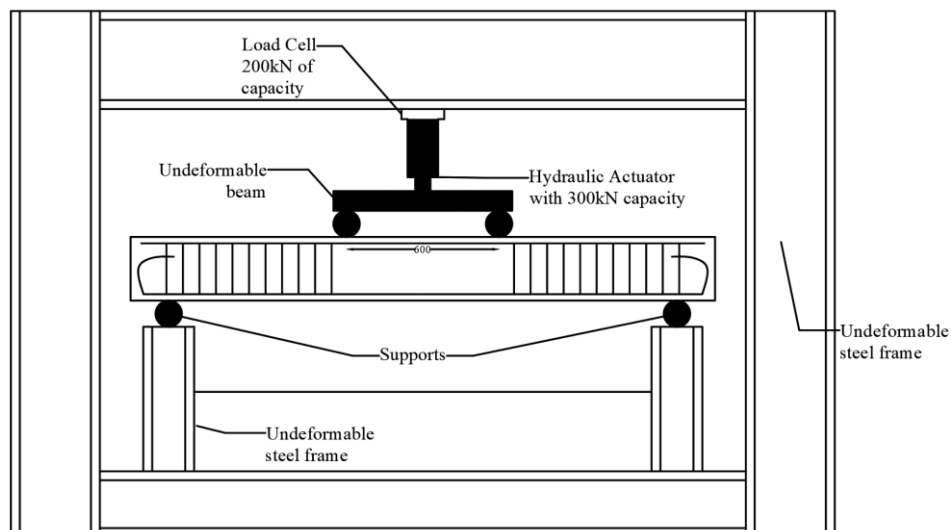


**Figure 6.** Bending test setup.

### 3. Results and Discussion

The data were analyzed based on the load-displacement curve and crack load–crack opening curve. These allow for both global and local behaviour.

The load displacement curves were analyzed to obtain a different global mechanical stage (cracking load, non-linear behavior, and failure). The different values for each stage are given in Table 5, with the load and midspan deflection corresponding to the first cracking, steel elastic limit strain, and failure.

**Table 5.** Representation of load and midspan deflection for key events during 4-point bending tests.

| Name | First Crack | | Steel Yielding | | Failure | |
|---|---|---|---|---|---|---|
| | Load [kN] | Deflection [mm] | Load [kN] | Deflection [mm] | Load [kN] | Deflection [mm] |
| R10-NR | 25 | 1.85 | 57.8 | 7.21 | 70.58 | 31.61 |
| R12-NR | 25 | 1.55 | 63.4 | 6.16 | 92.57 | 31.10 |
| R14-NR | 30 | 1.26 | 85.1 | 6.84 | 112.11 | 27.72 |
| R10-RB | 40 | 3.30 | 55.50 | 5.48 | 126.25 | 27.82 |
| R12-RB0 | 35 | 2.49 | 69.12 | 6.78 | 114.20 | 20.81 |
| R12-RB1 | 45 | 3.13 | 68.40 | 5.71 | 120.81 | 19.43 |
| R12-RB2 | 50 | 3.77 | 67.53 | 5.82 | 110.97 | 17.80 |
| R12-RB3 | 45 | 3.20 | 69.14 | 5.96 | 121.28 | 21.12 |
| R12-RB4 | 50 | 3.80 | 70.55 | 6.16 | 109.65 | 17.18 |
| R14-RB | 55 | 4.10 | 67.84 | 5.27 | 148.24 | 24.15 |

### 3.1. Ultimate Load

A CFRP external strengthening system allows for the modification of flexural behaviour in an RC beam in accordance with the literature review [35–40]. The increase in bending stiffness and/or ultimate bending moment is more effective for beams with a low steel ratio (0.4%). In this case, the ultimate capacity was increased by 80%. When the steel ratio is equal to 0.6% or 0.80% of the concrete section, the increase is given to be equal to 30%. Figure 7 demonstrates that ultimate load improvement was evident in the R10 beam, reaching almost 80% of the corresponding reference. By contrast, in the R12 and R14 groups, the ultimate load was not significantly different; both achieved a 30% improvement. Comparable results were obtained in the R12 group. The R12 and R14 group results were very close because the steel ratios (0.6% and 0.8%, respectively) were very close and the more the beam is already strengthened by longitudinal steel rebars the less FRP is efficient. The load–displacement curve clearly enhanced the effect of FRP on the ultimate load, as mentioned before. These results are comparable to those obtained by previous researchers; for example, Chajes et al. [41] shows that CFRP is more effective for load capacity increases than for increasing the stiffness.
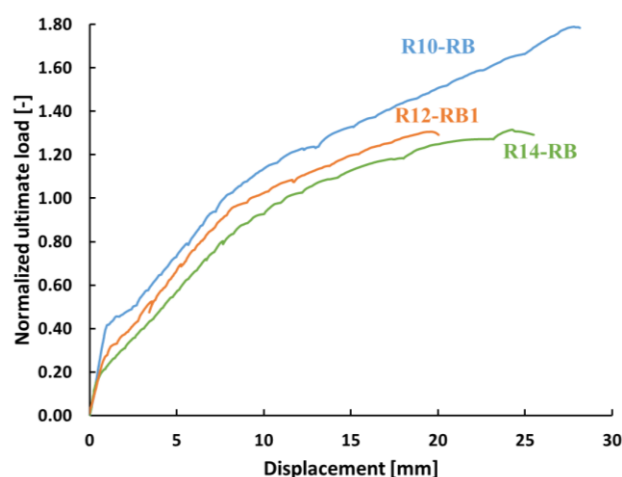


**Figure 7.** Improvement in ultimate load in the tested groups normalized to the reference one.

Since the design according to Eurocode 2 is based on behaviour governed by steel yielding and not on concrete crushing, the ultimate load of an RC beam is mostly dependent on the tensile capacity of the cross-section of the beam. The limit of the strengthening by externally bonded CFRP is the compressive strength of the top part of the beam to avoid concrete crush in compression zone.

### 3.2. Mid-Span Displacement

The strengthening using FRP modifies the bending stiffness of the beam because of externally bonded carbon fiber strengthening. Figure 8 enhances the load displacement curve, before the steel rebars yielding the bending stiffness is slightly increased by only 10%; at this stage, the bending stiffness value mainly depends on the concrete being under compression and the steel rebars being under tension. FRP contribution is low. Based on the cross-section on the beam, steel ratio, and FRP ratio reinforcement, the cracking inertia of the non-strengthened beam is around $93.10^6$ mm$^4$ while it grows to $116.10^6$ mm$^4$ when two layers of FRP are applied. When steel yields, its Young Modulus decreases to a low value, and, at this stage, all additional loss is undertaken by the CFRP and then the strengthening material is dependent on the highest second slope of the load displacement curve for the beams strengthened by CFRP. The R10-RB group exhibits a more significant improvement after strengthening. Therefore, the deflection is proportionally higher in the R10 beams. It is also important to outline that the more the beams are strengthened, the

more the ultimate deflection is reduced with a loss in beam ductility. This observation is linked to the failure mode of the beam with FRP debonding.
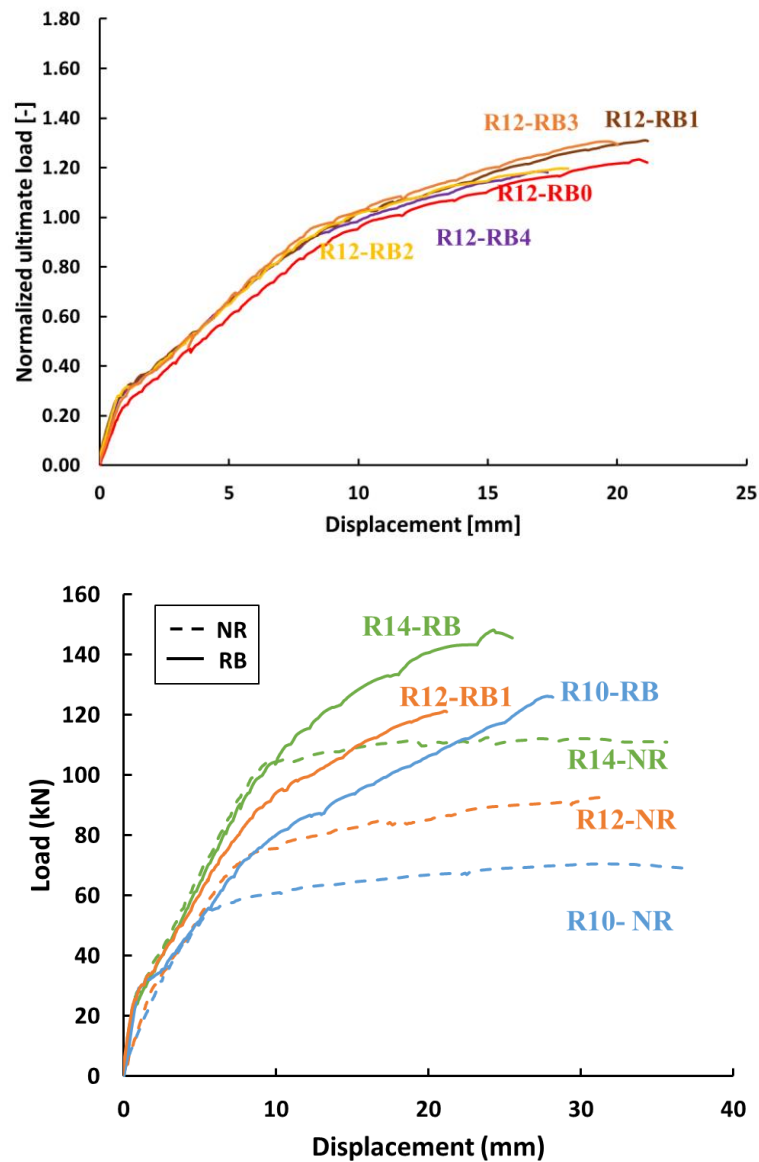


**Figure 8.** Reduction in deflection for the tested beams.

Composite Strain

In flexural strengthening, the task of the composite material is to increase the tensile strength of the section, which is partially guaranteed by the steel reinforcement. Knowledge of the stress level plays a crucial role in understanding the material's behaviour. For example, traction in the fiber produces shear stress within the resin used for bonding. An increase in the tangential stress is consequently the cause of the premature debonding of the reinforcement. Externally bonded fabric was applied on the concrete surfaces as presented in Section 2.2. The FRP is not prestressed before bonding and needs a crack to appear to develop tension [37].

In addition, due to the higher stiffness, when compared with the steel, the composite strain at a reference load is less than the corresponding steel strain. Similarly, as far as the influence of the steel ratio is concerned, due to what has been folded in the previous section, the composite is activated by reaching higher values in beams with less steel. Table 6 shows the difference in strain between steel and composite for several load levels for each test group. It can be seen that the composite exhibits more significant deformation than steel in

the early stages of loading. This inconsistency may be due to the strain gauge's positioning, which is not aligned with the correspondent placed on the steel bar.

**Table 6.** Comparison of strain between steel and composite for several load levels.

| Load [kN] | R10-RB | | R12-RB | | R14-RB | |
|---|---|---|---|---|---|---|
| | Steel Strain [µm/m] | Composite Strain [µm/m] | Steel Strain [µm/m] | Composite Strain [µm/m] | Steel Strain [µm/m] | Composite Strain [µm/m] |
| 10 | 19 | 22 | 58.19 | 70.46 | 63 | 68 |
| 35 | 1299 | 1696 | 1083 | 1350 | 1071 | 651 |
| 60 | 2730 | 2837 | 2112 | 2378 | 2132 | 1296 |
| 80 | 5433 | 4491 | 3314 | 3296 | 3020 | 1968 |
| 100 | 9798 | 7591 | 8257 | 6055 | 4398 | 2850 |
| 120 | 17,836 | 10,186 | - | - | 8379 | 4593 |
| 140 | - | - | - | - | 12,931 | 7161 |

### 3.3. Failure Modes

For all the strengthened beams using externally bonded CFRP, failure occurs during the debonding of the concrete covering at the end of the FRP layers near the beam support. This mode of failure is commonly called peeling-off in the literature. The shear stress in this area is located between the FRP and is caused when the steel longitudinal rebar is too high in comparison with the concrete tensile-shear strength (Figure 9).



**Figure 9.** Failure modes of strengthened beams.

### 3.4. Cracking Behaviour

The crack width was calculated thanks to the DIC method by obtaining images from a virtual displacement sensor located at 25 mm from the bottom right of the cracking zone. The displacement length of the displacement sensor was 1 cm so that the change in value was assumed to be only due to crack opening and not tensile concrete stress. The results were then analysed based on load–crack opening curves. The presence of CFRP fabric was found to influence the cracking behaviour of the tested beams, with a significant impact on the crack formation phase (CFP) [42,43]. Typically, when a crack appears, the effect of FRP allows to bridge the crack and limit the opening. For the cracking load, the FRP strain increased and controlled the tension in the steel rebars [44,45]. The load was transferred along the FRP bond length and when the load increased a new crack was initiated; this explained that the crack spacing was reduced [46]. In non-strengthened beams, the crack is

controlled around steel rebars in tension. Hognestad et al. [44] fixed the minimum value, $a_{min}$, given by Equation (1)

$$a_{min} = \frac{A_e f_t'}{u \Sigma o} \tag{1}$$

where $A_e$ is the effective area of concrete in tension, $f_t'$ is the concrete tensile strength, $u$ is the average bond stress, and $\Sigma o$ represents the sum of the bar perimeters.

In the experimental tests, strengthening further reduced the crack width in the R10 group compared with the other groups. The group with the lowest steel ratio exhibited a more significant effect at low-load levels. In fact, in the R10 group, steel yielding occurred at a lower load level, and the crack behaviour exhibited a divergent trend from 40 kN. However, the R12 and R14 groups did not exhibit consistent improvement in the first crack load because of the better steel–concrete adherence owing to the higher stiffness of the beam. In addition, the crack behaviour diverged for higher load values because of the later yielding of the steel bars (see Figure 10).
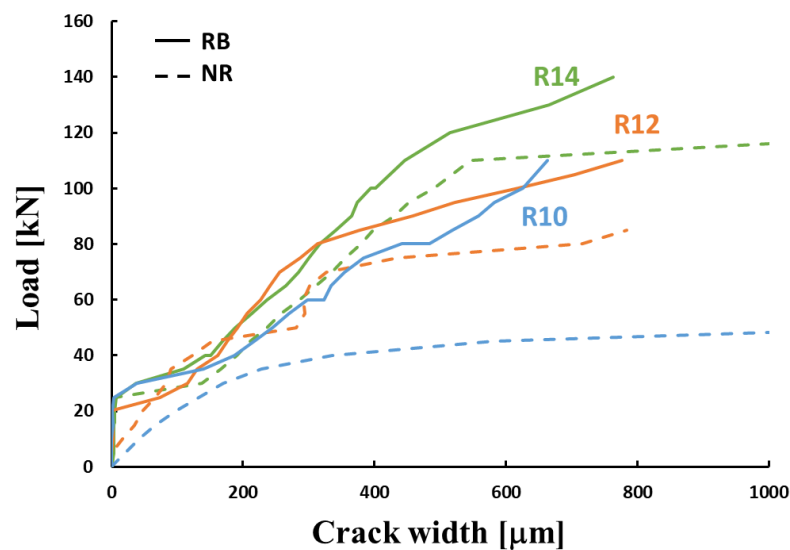


**Figure 10.** Crack–load curve.

A detailed overview of the crack width values for different load levels is provided in Table 7 and Figure 11.

**Table 7.** Values of crack opening values in function of loads.

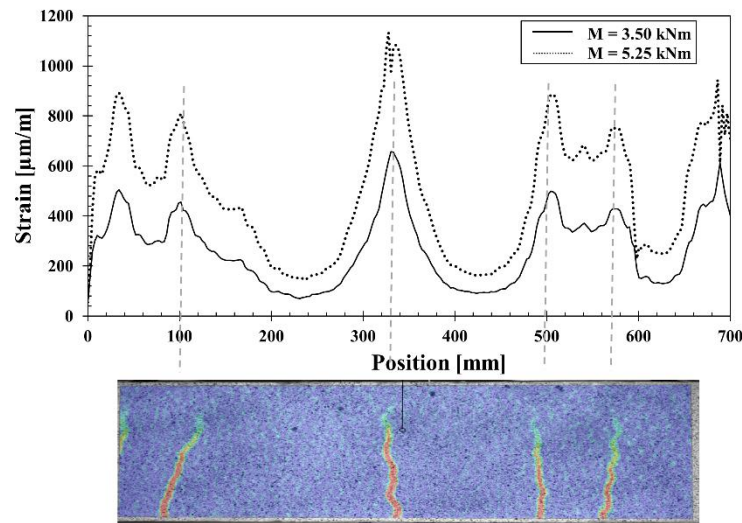| Load [kN] | Crack Width [μm] | | | | | |
|---|---|---|---|---|---|---|
| | **R10-NR** | **R12-NR** | **R14-NR** | **R10-RB** | **R12-RB1** | **R14-RB** |
| 25 | 133 | 124 | 137 | 3 | 72 | 7 |
| 30 | 169 | 145 | 166 | 7 | 115 | 37 |
| 40 | 334 | 190 | 210 | 33 | 161 | 142 |
| 50 | 1221 | 237 | 258 | 122 | 191 | 188 |
| 60 | - | 278 | 311 | 200 | 226 | 236 |
| 70 | - | 335 | 355 | 244 | 255 | 284 |
| 80 | - | 877 | 398 | 313 | 312 | 316 |
| 90 | - | - | 451 | 444 | 458 | 364 |
| 100 | - | - | 545 | 516 | 618 | 394 |
| 110 | - | - | - | - | 776 | 446 |
| 120 | - | - | - | - | - | 514 |

**Figure 11.** Evolution of strain and location of cracks for beams R10-RU80 for a bending moment of 3.5 and 5.25 kN·m based on DIC.

### 3.5. Model Proposal

Several codes have been proposed to predict bent RC crack spacing and the width of RC beams [24,47–49] under flexural loading. However, the presence of a strengthening system changes the usual crack behaviour, reducing the crack spacing and width [50,51]. The Eurocode 2 (EC2) model [24] is based on the principle of strain distribution between two adjacent cracks, between concrete and steel. The crack width is calculated as the product of the maximum spacing ($S_{r,max}$) and the steel–concrete mean strain difference ($\varepsilon_{sm} - \varepsilon_{cm}$), written as Equation (2).

$$w_k = S_{r,max} \cdot (\varepsilon_{sm} - \varepsilon_{cm}) \tag{2}$$

In this study, an EC2-modified model was proposed that considers the presence of a reinforcing system. The main hypothesis is that stress in steel rebar is reduced on the same level of load due to the hypothesis that the sum of the tensile force in a cross-section should be equal before and after strengthening under the same bending stiffness. Then the tensile strain in steel is also reduced. The simplicity of the model was maintained, and only a modification of the factor was presented to consider the effect of CFRP.

### 3.5.1. Eurocode Model

The EC2 formulation can predict the crack opening in an RC beam under a bending moment. The assumption is the relative difference between the steel strain and the concrete tensile strain before crack, and the difference is due to crack opening. The difference between the mean strains of the materials is based on a hypothesis of the perfect bonding of steel rebars with concrete. Then, a crack occurs when the steel strain is incompatible with the admitted concrete tensile strain [52]. EC2 provides a formula for calculating the mean strain difference between the RC constituent materials, depending on the geometrical and mechanical properties, given by Equation (3)

$$(\varepsilon_{sm} - \varepsilon_{cm}) = \left( \frac{\sigma_s - k_t \left( \frac{f_{ct,eff}}{\rho_{p,eff}} \right) \left( 1 + n\rho_{p,eff} \right)}{E_s} \right) \geq \frac{0.6\sigma_s}{E_s} \tag{3}$$

where $\sigma_s$ is the stress in the steel rebar, $f_{ct,eff}$ is the tensile concrete strength, $n$ is the steel–concrete elastic modulus ratio, $\rho_{p,eff}$ is the steel–concrete geometrical ratio referred to as the effective concrete area around the steel rebar $A_{c,eff}$, $E_s$ is the steel elastic modulus, and $k_t$ is a coefficient that considers the load duration (0.6 and 0.4 for short and long duration,

respectively). The value of $A_{c,eff}$ is also provided by EC2 with reference to the American Concrete Institute (ACI) [47] and is given by Equation (4)

$$A_{c,eff} = b_w Min\left\{2.5(h-d); \frac{h-x}{3}; 0.5h\right\} \tag{4}$$

Here, $h$ is the height of the cross-section, $d$ is the distance measured from the centroid of the steel reinforcement to the top concrete fiber, $b_w$ is the minimum section width, and $x$ is the neutral axis depth.

Meanwhile, the maximum crack spacing was calculated using Equation (5)

$$S_{r,max} = 3.4c + \frac{0.425k_1k_2k_4}{\rho_{p,eff}} \tag{5}$$

where $c$ is the concrete cover, $\phi$ is the reinforcing steel diameter, and $k_1$, $k_2$, and $k_4$ are the factors given by EC2.

The proposed equation fits the experimental data for the non-strengthened beams but is too conservative for beams strengthened using FRP. In particular, as illustrated in Figure 12, the EC2 formula is too conservative in the case of group R10, whereas it deviates less from the overall behaviour in the case of group R14, where the steel ratio is the highest. However, this result is understandable if one refers to Section 3.2, noting that the influence of the composite material was less evident in the group with a higher reinforcement level.
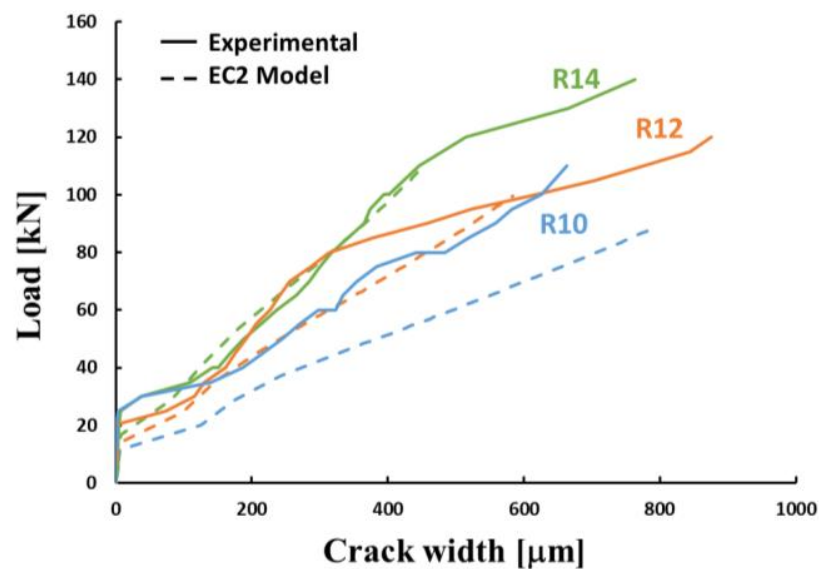


**Figure 12.** Comparison between experimental and predicted results using the existing EC2 formula.

3.5.2. Modified Model

The EC2 model accurately predicted the cracking evolution in an RC beam subjected to a bending moment. However, the increasing use of CFRP external strengthening of concrete structures highlights the need to adopt a new crack model for more extensive use by taking into consideration the strengthening effect. To consider the effect of strengthening by FRP and to input the geometrical and mechanical factors, a new relation was proposed that can better fit the model in this study. A new equation was proposed to modify the equation of steel strain (relation 6). The main objective was to introduce the effect of FRP on the changes in steel stress, to introduce the FRP cross-section in the equation, and to consider the modification of the neutral axis position due to FRP to obtain a better accuracy. The main objective was to introduce the geometrical properties of FRP in the model for design purposes.

The Young modulus of steel was modified to introduce FRP and a new model would consider the steel and composite moduli and material volume ratio. The homogenization factor $n^*$ was the ratio between the equivalent and concrete elastic moduli, and the geometrical reinforcement ratio. The percentage of tensile reinforcement was also modified to consider the effect of FRP $\rho_{p,eff}$ (relation (8)).

$$(\varepsilon_{sm} - \varepsilon_{cm})^* = \left( \sigma_s^* - \frac{k_t \left( \frac{f_{ct,eff}}{\rho_{p,eff}^*} \right) \left( 1 + n^* \rho_{p,eff}^* \right)}{E_r} \right) \geq \frac{0.6\sigma_s^*}{E_r} \tag{6}$$

$$E_r = \frac{E_s A_s + E_f A_f}{A_s + A_f} = \frac{E_s A_s + E_f A_f}{A_r} \tag{7}$$

$$\rho_{p,eff} = \frac{A_r}{A_{c,eff}} \tag{8}$$

Ceroni and Pecce [50] also modified the reinforcement ratio, which considers the use of CFRP written as Equation (9).

$$\rho_{p,eff} = \frac{A_s + \frac{A_f E_f}{E_s}}{A_{c,eff}} = \frac{A_s + n_f A_f}{A_{c,eff}} \tag{9}$$

The CFRP also modified the mechanical properties of the beam. Due to the addition of the tensile force on the bottom, the neutral axis position was changed to a lower position in comparison with non-strengthened beams. To calculate the new position of the neutral axis position, a numerical calculus process was proposed to obtain the neutral axis depth for each load level. At each step, compression and tensile forces were calculated to obtain the force cross-section equilibrium (10). The Bernoulli hypothesis and perfect bond between the steel and concrete was assumed. This allowed all strains to be written as functions of the steel strain (11). The material constitutive laws for concrete is linear-parabolic and the steel mechanical law is considered to be elastic-plastic, with an elastic behaviour for FRP. Therefore, three steps of calculation were undertaken: (i) all materials are elastic, (ii) concrete overpasses the pseudo-elastic range, and (iii) reinforcing steel yields.

The calculation process provided the assignment of steel strain. Then, starting from the geometrical centre $y_g$, a neutral axis depth was given, and the equilibrium was verified. A new neutral axis value was assigned if the section was not equilibrated. The flexural moment was calculated using the rotational equilibrium when the translational equilibrium was reached.

$$A_s \cdot E_s \cdot \varepsilon_s + A_f \cdot E_f \cdot \varepsilon_f = A_c \cdot E_c \cdot \varepsilon_c + A_s' \cdot E_s \cdot \varepsilon_s' \tag{10}$$

$$\frac{\varepsilon_s}{d - x} = \frac{\varepsilon_f}{H - x} = \frac{\varepsilon_c}{x} = \frac{\varepsilon_s'}{x - c} \tag{11}$$

The corrected neutral axis position changed the post-cracking behaviour of the beam cross-section because of the change in the damaged section inertia $I_{II}$, calculated as in (12). This value will change for each load level influencing the steel stress, calculated using Navier's Equation (13), where $M_{ser}$ is the flexural moment obtained from the rotational equilibrium, $I_I$ is the moment of inertia of the undamaged cross-section, and $M_{cr}$ is the flexural moment corresponding to the first cracking calculated using Equation (14) including the concrete mean tensile strength $f_{ctm}$.

$$I_{II} = \frac{b_w h^3}{3} + n A_s (d - x)^2 + n_f A_f (h - x)^2 \tag{12}$$

$$\sigma_s^* = \frac{n^* M_{ser}}{I_{II}} \cdot (d - x) + \frac{n^* M_{cr}}{I_I} \cdot (d - y_g) \tag{13}$$

$$M_{cr} = \frac{f_{ctm}}{y_g} \cdot I_I \tag{14}$$

The crack spacing value was determined using the same formulation reported in (5), substituting the $\rho_{p,eff}$ coefficient with the modified one.

The results accurately represent the crack behaviour until the steel yielded; however, the curve trend was linear rather than a double slope. Thus, the formulation was again modified to consider non-linear behaviour. The weight of the reinforcement materials (i.e., steel and concrete) in the equivalent elastic modulus following steel yielding was considered and discussed. Equation (7) was used in the steel elastic range and replaced with (15) following its yielding.

$$E_r = \frac{\alpha \cdot \sqrt{\beta} \cdot A_s \cdot E_s + A_f E_f}{A_f + A_s} \tag{15}$$

The $\beta$ factor considers potential damage in the beam after the first cracking and is the ratio between the first cracking moment $M_{cr}$ and the effective load at the time of verification $M_{ser}$. Finally, $\alpha$ had an experimental value of 2.1. As illustrated in Figure 13, the theoretical model predicted an earlier failure than the observed behaviour. However, because the cracking phenomenon mainly affected the service limit states, it was considered that assessing the accuracy of the empirical model up to theoretical failure was sufficient to describe the phenomenon. For each load level, a pair of crack width values were analysed to estimate the coefficient of determination $R^2$ and root mean square error (RMSE). The results are listed in Table 8 for each specimen group. In Figure 14, a comparison between the experimental- and model-obtained values is presented for the load level of 60 kN using the average value of the R12 series.
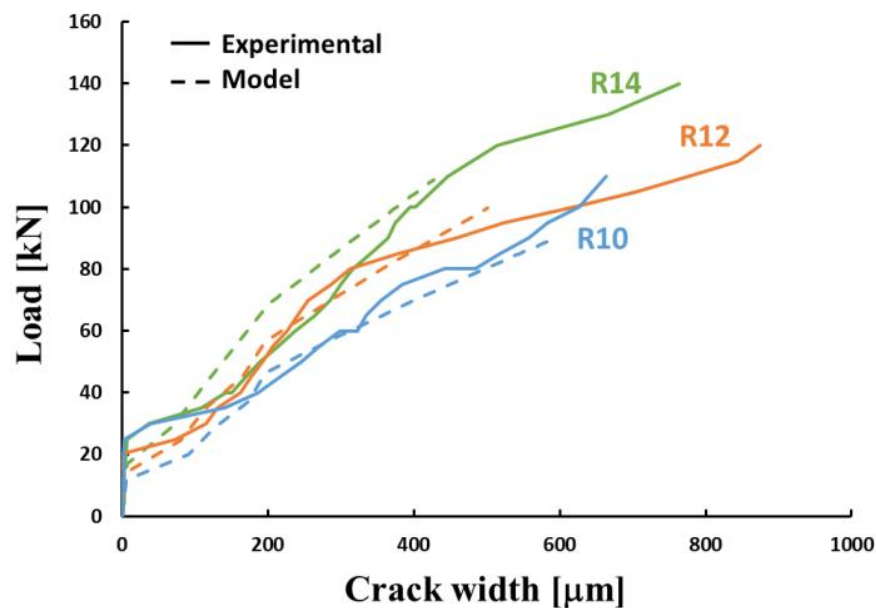


**Figure 13.** Comparison between the EC2-modified model and the experimental results.

**Table 8.** Coefficient of determination and root mean square error of the empirical model calculated for the tested groups.

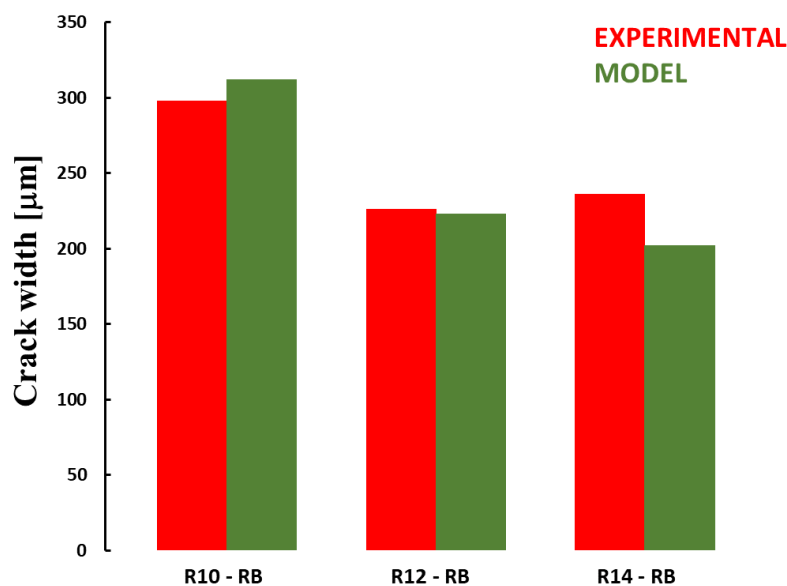| Group | R10 | R12 | R14 |
|:---:|:---:|:---:|:---:|
| $R^2$ | 0.85 | 0.96 | 0.98 |
| *RMSE* [μm] | 76.31 | 39.11 | 37.63 |

**Figure 14.** Comparison between the measured and calculated values of crack width corresponding to load level of 60 kN.

## 4. Conclusions

The present study aimed to evaluate the effect of externally bonded FRP on the cracking behaviour of reinforced concrete beams. Tests were undertaken on ten beams with three ratios of steel reinforcement and the FRP were reinforced by two layers of CFRP. The experimental results demonstrate the influence of the steel ratio on strength improvement, loss of ductility, and crack opening. The main results show that

- with a lower level of steel reinforcement, the contribution of the composite material was more significant.
- the beams with a low steel ratio (0.4%) suffered less loss in ductility and cracking.
- the crack opening calculation based on Eurocode 2 formula is too conservative compared with those measured.
- an empirical model was proposed based on the formulation of the Eurocode with appropriate modifications, taking into account the geometric and mechanical aspects of a strengthened structure. The calculated values were compared with the measured values and showed good agreement.

The presented model is proposed as an easy-to-use tool for design, allowing for the consideration of FRP for crack opening calculations. Future developments can be accomplished by comparing the model to others and comparing with other results from the literature review to validate this model and to introduce the effect of FRP on beams already damaged before strengthening. The model should also be extended to all kinds of FRP (laminate, higher or lower FRP ratio).

**Author Contributions:** Conceptualization, A.A. and L.M.; methodology, A.A.; software, A.A.; validation, M.S., L.M. and E.F.; resources, E.F.; writing—original draft preparation, E.F., A.A..; writing—review and editing, L.M.; supervision, L.M. and E.F. All authors have read and agreed to the published version of the manuscript.

## References

1. Maruyama, I.; Lura, P. Properties of early-age concrete relevant to cracking in massive concrete. *Cem. Concr. Res.* **2019**, *123*, 105770. [CrossRef]
2. Adamo, N.; Al-Ansari, N.; Sissakian, V.; Laue, J.; Knutsson, S. Dam Safety: Technical Problems of Ageing Concrete Dams. *J. Earth Sci. Geotech. Eng.* **2020**, *10*, 241–279.
3. Ahn, I.-S. Creep and Shrinkage of Early-Age Concrete at Cold Temperature. *Adv. Civ. Eng. Mater.* **2021**, *10*, 300–312. [CrossRef]
4. Wan-Wendner, R. Aging concrete structures: A review of mechanics and concepts. *Die Bodenkult. J. Land Manag. Food Environ.* **2018**, *69*, 175–199. [CrossRef]
5. Binda, L.; Tiraboschi, C.; Folli, R.T. On-site and Laboratory Investigation of Materials and Structure of a Belltower in Monza/Untersuchungen an den Werkstoffen und am Tragwerk im Labor und am Objekt am Beispiel eines Glockenturms in Monza. *Restor. Build. Monum.* **2000**, *6*, 41–62. [CrossRef]
6. Issa, M.; Ismail, E.-S. Long-term deflections of FRP reinforced concrete beams. *HBRC J.* **2020**, *16*, 269–282. [CrossRef]
7. Di Tommaso, A.; Neubauer, U.; Pantuso, A.; Rostasy, F. Behavior of Adhesively Bonded Concrete-CFRP Joints at Low and High Temperatures. *Mech. Compos. Mater.* **2001**, *37*, 327–338. [CrossRef]
8. Hu, C.; Sang, L.; Jiang, K.; Xing, J.; Hou, W. Experimental and numerical characterization of flexural properties and failure behavior of CFRP/Al laminates. *Compos. Struct.* **2021**, *281*, 115036. [CrossRef]
9. Bakis, C.E.; Bank, L.C.; Brown, V.L.; Cosenza, E.; Davalos, J.F.; Lesko, J.J.; Machida, A.; Rizkalla, S.H.; Triantafillou, T.C. Fiber-reinforced polymer composites for construction—State-of-the-art review. *J. Compos. Constr.* **2002**, *6*, 73–87. [CrossRef]
10. Nayak, A.N.; Kumari, A.; Swain, R.B. Strengthening of RC Beams Using Externally Bonded Fibre Reinforced Polymer Composites. *Structures* **2018**, *14*, 137–152. [CrossRef]
11. Peng, H.; Zhang, J.; Shang, S.; Liu, Y.; Cai, C.S. Experimental study of flexural fatigue performance of reinforced concrete beams strengthened with prestressed CFRP plates. *Eng. Struct.* **2016**, *127*, 62–72. [CrossRef]
12. Delle Ricerche, C.N. *Guide for the Design and Construction of Fiber-Reinforced Concrete Structures*; SN: CNR-DT; National Research Council-Advisory Committee on Technical Recommendations for Construction: Rome, Italy, 2006; Volume 204, p. 2006.
13. Triantafillou, T.; International Federation for Structural Concrete (Eds.) *Externally Bonded FRP Reinforcement for RC Structures: Technical Report on the Design and Use of Externally Bonded Fibre Reinforced Polymer Reinforcement (FRP EBR) for Reinforced Concrete Structures*; International Federation for Structural Concrete: Lausanne, Switzerland, 2001.
14. AFGC. Réparation et Renforcement des Structures en Béton au Moyen des Matériaux Composites. 2011. Available online: https://www.afgc.asso.fr/publication/reparation-et-renforcement-des-structures-en-beton-au-moyen-des-materiaux-composites/ (accessed on 1 February 2024).
15. Darby, A.; Ibell, T.; Clarke, J. *TR55 Design Guidance for Strengthening Concrete Structures Using Fibre Composite Materials*; The Concrete Society: Sandhurst, United Kingdom, 2004.
16. *SIA166*; Klebebewehrungen (Externally Bonded Reinforcements. Schweizer I. Architektenverein: Zürich, Switzerland, 2004.
17. ACI Committee 440. *440.2R-17: Guide for the Design and Construction of Externally Bonded FRP Systems for Strengthening Concrete Structures*; American Concrete Institute: Farmington Hills, MI, USA, 2017. [CrossRef]
18. Gorbunov, I.; Kakusha, V. Behavior of concrete beams reinforced with FRP during bending. *E3S Web Conf.* **2021**, *263*, 02052. [CrossRef]
19. del Rey Castillo, E.; Allen, T.; Henry, R.; Griffith, M.; Ingham, J. Digital image correlation (DIC) for measurement of strains and displacements in coarse, low volume-fraction FRP composites used in civil infrastructure. *Compos. Struct.* **2019**, *212*, 43–57. [CrossRef]
20. Zhou, K.; Lei, D.; Chun, P.-j.; She, Z.; He, J.; Du, W.; Hong, M. Evaluation of BFRP strengthening and repairing effects on concrete beams using DIC and YOLO-v5 object detection algorithm. *Constr. Build. Mater.* **2024**, *411*, 134594. [CrossRef]
21. Armonico, A.; Saidi, M.; Michel, L.; Bel, S.; Ferrier, E. Inverse analysis based on DFOS technology for the study of the bonding behaviour of FRP to concrete beams. *Mater. Today Commun.* **2023**, *35*, 105655. [CrossRef]
22. Hoult, N.A.; Andy Take, W.; Lee, C.; Dutton, M. Experimental accuracy of two dimensional strain measurements using Digital Image Correlation. *Eng. Struct.* **2013**, *46*, 718–726. [CrossRef]
23. Mehdikhani, M.; Aravand, M.; Sabuncuoglu, B.; Callens, M.G.; Lomov, S.V.; Gorbatikh, L. Full-field strain measurements at the micro-scale in fiber-reinforced composites using digital image correlation. *Compos. Struct.* **2016**, *140*, 192–201. [CrossRef]
24. *Eurocode 2: Design of Concrete Structures—Part 1-1: General Rules and Rules for Buildings*; European Union: Brussels, Belgium, 2004; p. 230.
25. *BS EN 12390-3:2009*; Testing Hardened Concrete. Compressive Strength of Test Specimens. British Standards Institution: London, UK, 2009.
26. *ISO 527-5:2021*; Plastics—Determination of Tensile Properties—Part 5: Test Conditions for Unidirectional Fibre-Reinforced Plastic Composites. ISO: Geneva, Switzerland, 2021; Volume 5.
27. Sutton, M.A.; Orteu, J.J.; Schreier, H. *Image Correlation for Shape, Motion and Deformation Measurements: Basic Concepts, Theory and Applications*; Springer Science & Business Media: Berlin/Heidelberg, Germany, 2009.
28. Pan, B.; Qian, K.; Xie, H.; Asundi, A. Two-dimensional digital image correlation for in-plane displacement and strain measurement: A review. *Meas. Sci. Technol.* **2009**, *20*, 062001. [CrossRef]

29. International Digital Image Correlation Society. *A Good Practices Guide for Digital Image Correlation*; International Digital Image Correlation Society (iDICs): Boston, MA, USA, 2018.

30. Tehrani, A.D.; Kohankar Kouchesfehani, Z.; Najafi, M. Pipe profiling using digital image correlation. In *Pipelines 2020*; American Society of Civil Engineers Reston: Reston, VA, USA, 2020; pp. 36–45.

31. Saidi, M.; Gabor, A. Use of distributed optical fibre as a strain sensor in textile reinforced cementitious matrix composites. *Measurement* **2019**, *140*, 323–333. [CrossRef]

32. Bravo, M.; Sáenz, J.; Navas, M.; Lopez-Amo, M. Concrete Beam Bending Test Monitorization Using a High Strain Fiber Optic Sensor. *J. Light. Technol.* **2012**, *30*, 1085–1089. [CrossRef]

33. Ferrier, E.; Caggegi, C.; Michel, L. Influence of EB-CFRP on Cracks for Reinforced Concrete Beams Strengthening. *Spec. Publ.* **2018**, *237*, 44.1–44.16.

34. Yusra, A.; Opirina, L.; Triwulan, T.; Raka, G.; Safriani, M. Comparative Study of Steel Reinforced Concrete Beams with Bamboo Reinforced Concrete Beams. *Solid State Technol.* **2021**, *63*, 12857–12863.

35. Banjara, N.K.; Ramanjaneyulu, K. Investigations on behaviour of flexural deficient and CFRP strengthened reinforced concrete beams under static and fatigue loading. *Constr. Build. Mater.* **2019**, *201*, 746–762. [CrossRef]

36. Shamass, R.; Mahi, B.; Cashell, K.A.; Abarkan, I.; El-Khannoussi, F. Experimental investigation into the behaviour of continuous concrete beams reinforced with basalt FRP. *Eng. Struct.* **2022**, *255*, 113888. [CrossRef]

37. Al-Khafaji, A.; Salim, H.; El-Sisi, A. Behavior of RC beams strengthened with CFRP sheets under sustained loads. *Structures* **2021**, *33*, 4690–4700. [CrossRef]

38. Ali, H.; Assih, J.; Li, A. Flexural capacity of continuous reinforced concrete beams strengthened or repaired by CFRP/GFRP sheets. *Int. J. Adhes. Adhes.* **2020**, *104*, 102759. [CrossRef]

39. Bocciarelli, M.; di Feo, C.; Nisticò, N.; Pisani, M.A.; Poggi, C. Failure of RC beams strengthened in bending with unconventionally arranged CFRP laminates. *Compos. Part B Eng.* **2013**, *54*, 246–254. [CrossRef]

40. Pisani, M. Evaluation of Bending Strength of RC Beams Strengthened with FRP Sheets. *J. Compos. Constr.* **2006**, *10*, 313–320. [CrossRef]

41. Chajes, M.J.; Thomson, T.A., Jr.; Januszka, T.F.; Finch, W.W., Jr. Flexural strengthening of concrete beams using externally bonded composite materials. *Constr. Build. Mater.* **1994**, *8*, 191–201. [CrossRef]

42. Euro-International Committee for Concrete; Favre, R. *CEB Design Manual on Cracking and Deformations*; École Polytechnique Fédérale de Lausanne: Lausanne, Switzerland, 1985.

43. Ng, P.L.; Kwan, A. A rigorous analytical model for shrinkage cracking of reinforced concrete. *Mag. Concr. Res.* **2017**, *69*, 120–133. [CrossRef]

44. Hognestad, E. High-strength bars as concrete reinforcement, Part 2: Control of flexural cracking. *J. PCA Res. Dev. Lab.* **1962**, 46–53.

45. Watstein, D.; Parsons, D.E. Width and spacing of tensile cracks in axially reinforced concrete cylinders. *J. Res. Natl. Bur. Stand.* **1943**, *31*, 1–24. [CrossRef]

46. Borosnyói, A.; Balázs, G.L. Models for flexural cracking in concrete: The state of the art. *Struct. Concr.* **2005**, *6*, 53–62. [CrossRef]

47. *ACI 318R-08*; Building Code Requirements for Structural Concrete (ACI 318-08) and Commentary: An ACI Standard. American Concrete Institute (ACI): Farmington Hills, MI, USA, 2008.

48. *ECP 203-2007*; Egyptian Code for Design and Construction of Reinforced Concrete Structures. Ministry of Housing, Utilities and Urban Communities: El Sayeda Zeinab, Egypt, 2007.

49. *BS 8110-2:1985*; Structural Use of Concrete. Part 2: Code of Practice for Special Circumstances. British Standards Institution: Milton Keynes, UK, 1985.

50. Ceroni, F.; Pecce, M. Design provisions for crack spacing and width in RC elements externally bonded with FRP. *Compos. Part B Eng.* **2009**, *40*, 17–28. [CrossRef]

51. Barris, C.; Torres, L.; Vilanova, I.; Miàs, C.; Llorens, M. Experimental study on crack width and crack spacing for Glass-FRP reinforced concrete beams. *Eng. Struct.* **2017**, *131*, 231–242. [CrossRef]

52. Leonhardt, F. *Crack Control in Concrete Structures*; PCI Journal: Chicago, IL, USA, 1977.